

Newborn spheroids at high redshift: when and how did the dominant, old stars in today’s massive galaxies form?

S. Kaviraj^{1,2,3}, S. Cohen⁴, R. S. Ellis³, S. Peirani⁵, R. A. Windhorst⁴,
R. W. O’Connell⁶, J. Silk^{5,2}, B. C. Whitmore⁷, N. P. Hathi⁸, R. E. Ryan Jr⁷,
M. A. Dopita^{9,10}, J. A. Frogel^{10,11} and A. Dekel¹²

¹Blackett Laboratory, Imperial College London, London SW7 2AZ, UK

²Department of Physics, University of Oxford, Keble Road, Oxford, OX1 3RH, UK

³California Institute of Technology, 105-24 Astronomy, Pasadena, CA 91125, USA

⁴School of Earth and Space Exploration, Arizona State University, Tempe, AZ 85287-1404, USA

⁵Institut d’Astrophysique de Paris, 98 bis boulevard Arago, 75014 Paris

⁶Department of Astronomy, University of Virginia, Charlottesville, VA 22904-4325, USA

⁷Space Telescope Science Institute, Baltimore, MD 21218, USA

⁸Carnegie Observatories, 813 Santa Barbara Street, Pasadena, California, 91101, USA

⁹Research School of Physics and Astronomy, The Australian National University, ACT 2611, Australia

¹⁰King Abdulaziz University, Astronomy Department, Faculty of Science, Jeddah, Saudi Arabia

¹¹Galaxies Unlimited, 1 Tremblant Court, Lutherville, MD 2109 USA

¹²Racah Institute of Physics, The Hebrew University, Jerusalem 91904, Israel

8 March 2013

ABSTRACT

We study ~ 330 massive ($M_* > 10^{9.5} M_\odot$), newborn spheroidal galaxies (SGs) around the epoch of peak star formation ($1 < z < 3$), to explore the high-redshift origin of SGs and gain insight into when and how the old stellar populations that dominate today’s Universe formed. The sample is drawn from the HST/WFC3 Early-Release Science programme, which provides deep 10-filter ($0.2 - 1.7 \mu\text{m}$) HST imaging over a third of the GOODS-South field. We find that the star formation episodes that built our SGs likely peaked in the redshift range $2 < z < 5$ (with a median of $z \sim 3$) and have decay timescales shorter than ~ 1.5 Gyr. Starburst timescales and ages show no trend with stellar mass in the range $10^{9.5} M_\odot < M_* < 10^{10.5} M_\odot$. However, the timescales show increased scatter towards lower values (< 0.3 Gyr) for $M_* > 10^{10.5} M_\odot$, and an age trend becomes evident in this mass regime: SGs with $M_* > 10^{11.5} M_\odot$ are ~ 2 Gyrs older than their counterparts with $M_* < 10^{10.5} M_\odot$. Nevertheless, a *smooth* downsizing trend with galaxy mass is not observed, and the large scatter in starburst ages indicates that SGs are not a particularly coeval population. Around half of the *blue* SGs appear not to drive their star formation via major mergers, and those that have experienced a recent major merger, show only modest enhancements ($\sim 40\%$) in their specific star formation rates. Our empirical study indicates that processes other than major mergers (e.g. violent disk instability driven by cold streams and/or minor mergers) likely play a dominant role in building SGs, and creating a significant fraction of the old stellar populations that dominate today’s Universe.

Key words: galaxies:formation – galaxies:evolution – galaxies: high-redshift – galaxies: elliptical and lenticular, cD – galaxies: interactions

1 INTRODUCTION

Massive galaxies are central to our understanding of the visible Universe. Locally, the massive galaxy census is dominated by systems with spheroidal morphology. Hosting more than $\sim 50\%$ of the stellar mass at the present day (e.g. Bernardi et al. 2003), these massive spheroidal galax-

ies (SGs) are key laboratories for studying the evolution of galaxies over cosmic time. Their red optical colours (e.g. Bower et al. 1992; Ellis et al. 1997; Stanford et al. 1998; Gladders et al. 1998; Bernardi et al. 2003; Bell et al. 2004; Kaviraj et al. 2005; Faber et al. 2007), obedience of a ‘fundamental plane’ with little intrinsic scatter

(e.g. Jorgensen et al. 1996; Franx 1995; Saglia et al. 1997; Forbes et al. 1998; Peebles 2002) and chemical evidence for short star-formation timescales (e.g. Trager et al. 2000; Thomas et al. 2005), indicate that the bulk of their stellar mass formed rapidly at high redshift ($z > 1$). Nevertheless, the young (luminosity-weighted) ages observed in some SGs are a signature of recent (< 5 Gyr) star formation (e.g. Ellis et al. 2001; Menanteau et al. 2001; Nelan et al. 2005; Schiavon 2007; Trager et al. 2008; Graves et al. 2009), which can be accurately quantified using a sensitive probe of young stars, such as the rest-frame ultraviolet (UV; 1200-3000 Å). Recent UV studies have shown that, while old stars do dominate today’s SGs, a significant minority ($\sim 20\%$) of the stellar mass in these galaxies is formed at $z < 1$ (Kaviraj et al. 2007a; 2008, see also Ferreras & Silk 2000a; Yi et al. 2005; Salim & Rich 2010; de la Rosa et al. 2011; Rutkowski et al. 2012), via minor mergers between SGs and gas-rich dwarfs (Kaviraj et al. 2009a; Kaviraj et al. 2011, see also Tal et al. 2012; Newman et al. 2011).

While it is clear that the dominant stellar populations in SGs are old, remarkably little is known about exactly when and how these stars formed in the early Universe. The key questions are: (1) *At what redshifts and over what timescales did they form?* (2) *What were the principal mechanisms that drove this star formation?* While the former question has been explored using spectro-photometric studies of local SGs, it is challenging to construct a detailed star formation history for the old stars using *local* SGs, because the available spectro-photometric indicators are insensitive to old stellar populations of different ages. Optical colours, for example, evolve slowly after 4-5 Gyr (e.g. Yi 2003). A further complication is that *all* indicators are affected by recent star formation, typically by an uncertain amount in any given galaxy. While old stellar populations do dominate SGs *by mass*, measured spectro-photometric quantities are *luminosity-weighted*. Since the luminosity-weighting of young stars is higher than their old counterparts, even small amounts of recent star formation can have a disproportionately large impact on the indicator in question. Thus, while it is possible to put lower limits on the age of the old stellar populations in today’s SGs, the exact shape of the star formation history of these old stars remains elusive. It is worth noting that the *average timescale* of star formation in individual galaxies can be estimated with reasonable precision using $[\alpha/\text{Fe}]$ ratios¹. Indeed, the super-solar $[\alpha/\text{Fe}]$ ratios observed in most SGs suggest star-formation timescales less than ~ 1 Gyr (Trager et al. 2000; Ferreras & Silk 2000b; Thomas et al. 2005).

The latter question (2) has been the focus of some debate in the literature. While the classical view has been that SGs are products of ‘major’ (roughly equal-mass) mergers between massive spiral galaxies in the early Universe (e.g. Toomre 1977; White 1978; Barnes & Hernquist 1992; Somerville & Primack 1999;

¹ α elements are primarily provided by prompt Type II supernovae, which explode almost instantaneously ($\sim 10^6$ yr) on cosmological timescales. Fe, on the other hand, is provided by Type Ia supernovae (SN), which emerge after typical time delays of less than a Gyr (e.g. Thomas et al. 1999). The $[\alpha/\text{Fe}]$ ratio therefore indicates the ratio of the overall timescale of star formation in a galaxy to the onset timescale of the Type Ia SN.

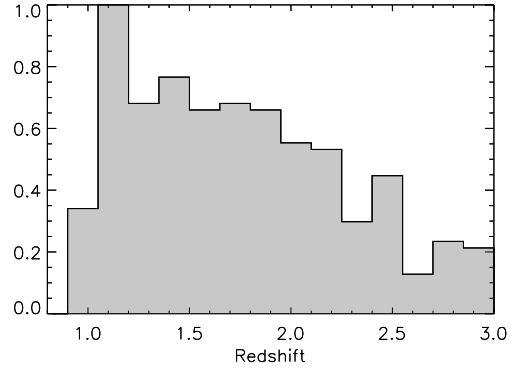


Figure 1. Redshift distribution of the SGs in this study.

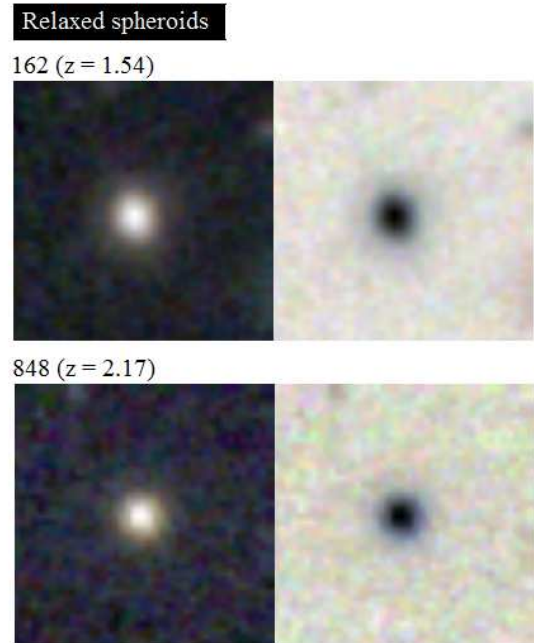


Figure 2. Examples of relaxed SGs in our dataset. The redshift of each galaxy is indicated above the image, next to its ID. We show both the *YJH* colour image and its negative.

Cole et al. 2000; Hatton et al. 2003; Springel et al. 2005), recent hydrodynamical simulations (e.g. Dekel et al. 2009; Kereš et al. 2009; Devriendt et al. 2010), coupled with the observed paucity of major mergers at high redshift (e.g. Genzel et al. 2008; Law et al. 2009; Jogee et al. 2009; Kaviraj et al. 2011), suggest that the progenitors of SGs may not predominantly be major mergers but rather clumpy disks, in which star formation is fed by cold streams and minor mergers (see e.g. Birnboim & Dekel 2003; Kereš et al. 2005; Dekel et al. 2009; Ceverino et al. 2010, 2012), with the clumps eventually coalescing to form a spheroid.

Given these significant open issues, a detailed *empirical* understanding of the formation of the dominant, old stars in today’s SGs is highly desirable, both as a route to understanding the drivers of star formation in the early

Universe, and as an important test of our emerging theoretical models for the high-redshift Universe. Given the limited utility of local SGs in studying these issues, an ideal method for probing questions (1) and (2) above is to study *newborn* SGs around the epoch of peak cosmic star formation ($1 < z < 3$, see Madau et al. 1998; Hopkins 2004; Hopkins & Beacom 2006). Quantifying the star formation histories of these systems then allows us to directly probe the formation of the old stars in today’s SGs, free from the contamination of the galaxy spectrum by intervening star formation episodes at late epochs. The underlying assumption is that newborn SGs at high redshift are the ancestors of their present-day counterparts, i.e. that SGs do not routinely transform into disks over cosmic time. Both theoretical and observational work on the evolving morphological mix of the Universe suggests that this is indeed a reasonable assumption to make (e.g. Butcher & Oemler 1984; Baugh et al. 1996; Couch et al. 1998; Smith et al. 2005).

While the analysis of newborn SGs at $z > 1$ is a compelling project, past studies of statistically large samples of SGs (e.g. Ferreras et al. 2009) have typically fallen short of this epoch, because deep, *survey-scale* HST imaging in the near-infrared (NIR), required for obtaining rest-frame optical galaxy morphologies at $z > 1$, has, until recently, been lacking. However, following the GOODS-NICMOS survey (Conselice et al. 2011), a new generation of NIR surveys using the HST’s WFC3 – e.g. the WFC3 Early-Release Science (ERS) programme (Windhorst et al. 2011) and the ongoing CANDELS campaign (Koekemoer et al. 2011; Grogin et al. 2011) – are providing unprecedented large-scale access to rest-frame optical galaxy data at $z > 1$, making them ideal datasets for the study of newborn SGs at high redshift. Here, we employ WFC3 ERS data and study SGs around the epoch of peak cosmic star formation, to explore the high-redshift origin of these galaxies and gain insight into when and how the old stellar populations that dominate today’s Universe formed. We leverage the unprecedentedly deep NIR imaging to morphologically identify SGs and explore the role of major mergers in their evolution, and exploit the uniquely wide ERS wavelength baseline ($0.2 - 1.7 \mu\text{m}$) to quantify galaxy star formation histories via the available rest-frame UV-optical photometry.

This paper is organised as follows. In Section 2, we briefly describe the ERS dataset and the morphological selection of SGs using visual inspection. In Section 3, we describe the calculation of star formation histories and rest-frame photometry for individual SGs in our sample. In Section 4, we study the photometric properties of the newborn SGs, use their derived star formation histories to constrain the formation epoch of their stellar mass and explore the mechanisms by which this stellar mass is likely being formed. We summarise our findings and outline avenues for future work in Section 5. Throughout this paper we use the WMAP7 cosmological parameters (Komatsu et al. 2011). All photometry is presented in the AB system (Oke & Gunn 1983).

2 GALAXY SAMPLE AND MORPHOLOGICAL CLASSIFICATION

Disturbed spheroids

1296 ($z = 1.65$)



949 ($z = 2.45$)



1047 ($z = 1.58$)



3434 ($z = 1.81$)



Figure 3. Examples of disturbed SGs in our dataset. The redshift of each galaxy is indicated above the image, next to its ID. We show both the YJH colour image and its negative.

The WFC3 ERS programme has imaged around one-third of the GOODS-South field with both the UVIS and IR channels of the HST/WFC3. The observations, data reduction, and instrument performance are described in detail in Windhorst et al. (2011), and highlighted here. The goal of this part of the ERS programme was to demonstrate the science capabilities of the WFC3 for studying intermediate- and high-redshift galaxies in both the UV and NIR, by observing a portion of the well-studied GOODS-South field (Giavalisco et al. 2004). The field was observed for 104 orbits, with 40 orbits in the UVIS channel and 60 orbits in the NIR channel. The UVIS data covered $\sim 55 \text{ arcmin}^2$, in

	$1 < z < 1.5$		$1.5 < z < 3$	
	f_{SG}	$N_{\text{DSG}}/N_{\text{SG}}$	f_{SG}	$N_{\text{DSG}}/N_{\text{SG}}$
$\text{Log } M_* > 9.5$	0.35 ± 0.02	0.42 ± 0.04	0.32 ± 0.02	0.35 ± 0.04
$9.5 < \text{Log } M_* < 11$	0.36 ± 0.03	0.43 ± 0.05	0.36 ± 0.02	0.36 ± 0.04
$\text{Log } M_* > 11$	0.56 ± 0.11	0.33 ± 0.12	0.58 ± 0.13	0.18 ± 0.08

Table 1. The fraction of galaxies that are SGs (f_{SG}) in various stellar mass (units of M_\odot) and redshift ranges, and the fraction *within* the SGs that are disturbed ($N_{\text{DSG}}/N_{\text{SG}}$). For the most massive galaxies ($10^{11}M_\odot$ - $10^{12}M_\odot$), for example, the fraction of SGs is $\sim 60\%$, similar to the value found by Cameron et al. 2011, who also employed visual inspection for identifying ETGs. The total number of galaxies in this study is 818 (736 in the range $9.5 < \text{Log } M_* < 11$ and 82 with $\text{Log } M_* > 11$).

each of the F225W, F275W and F336W filters, with relative exposure times of 2:2:1. The IR data covered $\sim 45 \text{ arcmin}^2$ using the F098M (Y_s), F125W (J), and F160W (H) filters with equal exposure times of 2 orbits per filter. The data were astrometrically aligned with a version of the GOODS-S HST/ACS data (v2.0²; Giavalisco et al. 2004) that was rebinned to have a pixel scale of $0''.09$ per pixel. Together, the data provide 10-band HST panchromatic coverage over $0.2 - 1.7 \mu\text{m}$, with a 5σ point-source depth of $AB \sim 26.4$ mag in the UV and $AB \sim 27.5$ mag in the IR.

Our focus in this paper is the subset of 818 ERS galaxies that have either spectroscopic or photometric redshifts in the range $1 < z < 3$. Photometric redshifts are calculated using the EAZY code (Brammer et al. 2008) on the 10-band WFC3/ACS photometric catalogue (Cohen et al. in prep). Spectroscopic redshifts are drawn from the literature, from spectra taken using the Very Large Telescope (Le Fèvre et al. 2004; Szokoly et al. 2004; Mignoli et al. 2005; Ravikumar et al. 2007; Vanzella et al. 2008; Popesso et al. 2009), the Keck telescopes (Strolger et al. 2004) and the HST ACS grism (Daddi et al. 2005; Pasquali et al. 2006; Ferreras et al. 2009). For the analysis that follows (e.g. in Section 3), spectroscopic redshifts are always used where available. Figure 1 shows the redshift distribution of the SG sample in this study.

Each galaxy in this sample is morphologically classified via visual inspection of its WFC3/NIR images, which trace the rest-frame optical wavelengths at $z > 1$. While morphological proxies, such as concentration, asymmetry, clumpiness, M_{20} and the Gini coefficient have been widely used to classify galaxies in large surveys (see e.g. Abraham et al. 1996, 2003; Conselice et al. 2003; Lotz et al. 2004), the performance of these methods is typically calibrated against visual inspection (e.g. Abraham et al. 1996), which offers better precision and reliability in morphological classification (e.g. Lisker 2008; Robaina et al. 2009; Kartaltepe et al. 2010). Past HST studies of the high-redshift Universe (including recent efforts using the WFC3) have commonly exploited visual inspection to classify galaxy morphologies (e.g. Elmegreen et al. 2005; Ferreras et al. 2005; Bundy et al. 2005; Cassata et al. 2005; Jogee et al. 2009; Robaina et al. 2009; Kaviraj et al. 2011; Cameron et al. 2011; Kocevski et al. 2012), using rest-frame optical imaging that has similar or fainter surface-brightness limits compared to the images employed here.

In this paper, we visually inspect YJH composite im-

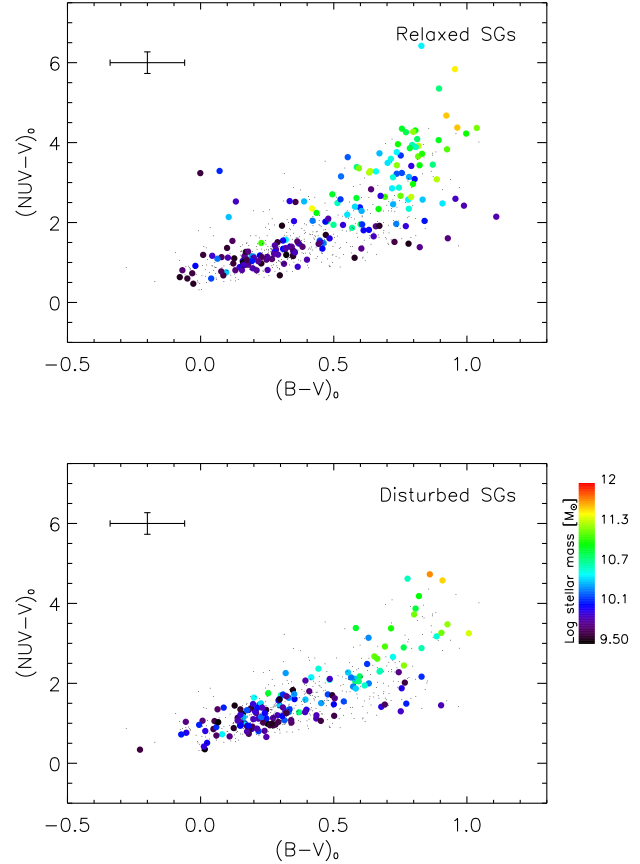


Figure 4. Rest-frame UV/optical colours of the ERS galaxies in the redshift range $1 < z < 3$. The top panel shows SGs that are relaxed i.e. do not show any morphological disturbances, while the bottom panel shows SGs that are morphologically disturbed. The filled coloured circles represent SGs, while the small black dots represent late-type galaxies. The colour coding indicates the stellar mass of the SG (see legend). The errors in the stellar masses are typically better than 0.3 dex.

ages, scaled using the asinh method of Lupton et al. (2004), to determine (1) the morphology of the galaxy and (2) whether it exhibits morphological disturbances, i.e. tidal features indicative of a recent merger. Using YJH composites (instead of monochrome images in one filter) maximises the rest-frame optical information in the image, and facilitates the identification of tidal features. While previous studies have successfully performed visual inspection

² <http://archive.stsci.edu/pub/hlsp/goods/v2/>

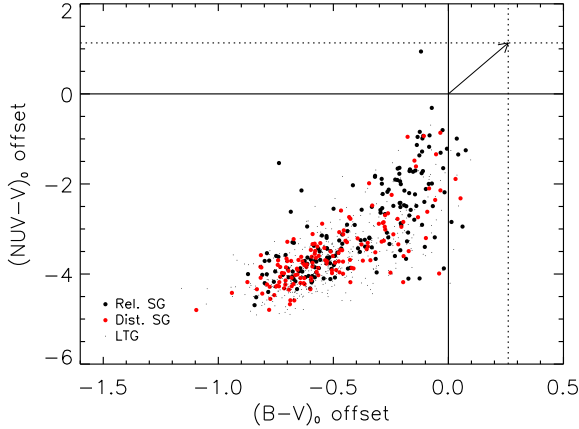


Figure 5. The *offset* between the rest-frame colours of individual SGs and that of a dustless, solar-metallicity instantaneous burst at $z = 5$. The dotted line shows how the offset will change if we consider a more realistic instantaneous burst that is folded with the median value for the internal extinction of the SGs ($E_{B-V} \sim 0.2$ mag). The arrow indicates the reddening vector for this extinction value. Black and red circles indicate relaxed and disturbed SGs respectively and small black dots indicate late-type galaxies. This comparison, intended only as a guide, indicates that none of the SGs in our sample are likely to have completed their stellar mass assembly by $z \sim 5$.

of similar datasets to $H \sim 25$ mag (e.g. Cameron et al. 2011), we restrict our galaxy sample to a more conservative $H \sim 24.5$ mag (in this magnitude range the galaxy sample with $M_* > 10^{9.5} M_\odot$ is expected to be complete; Windhorst et al. 2011). Galaxies are classified into two morphological classes: SGs and a (broad) class of ‘late-types’, which includes all objects that are not spheroidal, e.g. disks, clumpy galaxies, irregulars, etc. Here, we focus solely on the SGs, splitting them into ‘relaxed’ systems, which do not exhibit morphological disturbances indicative of recent interactions, and ‘disturbed’ systems, which do (see Figures 2 and 3 for examples of relaxed and disturbed SGs respectively). The visual classification process identifies 328 SGs in our sample. As we describe in Section 4 below, the disturbed SGs are likely to have experienced recent *major* mergers.

For the analysis that follows, we study ERS galaxies that have redshifts in the range $1 < z < 3$, H -band magnitudes brighter than 24.5 (where morphologies are reliable) and stellar masses greater than $10^{9.5} M_\odot$ (the derivation of stellar masses is described in Section 3 below). Table 1 summarises the fraction of galaxies that are SGs (f_{SG}) in various stellar mass and redshift ranges and the fraction *within* the SGs that are disturbed ($N_{\text{DSG}}/N_{\text{SG}}$). For example, for the most massive galaxies ($M_* > 10^{11} M_\odot$), the fraction of SGs is $\sim 60\%$, similar to the value found by Cameron et al. (2011), who also used visual inspection of WFC3 images for morphological classification. In the mass range considered here ($M_* > 10^{9.5} M_\odot$), around a third of SGs exhibit morphological disturbances. The disturbed fraction decreases with increasing redshift, plausibly due to greater cosmological dimming of the tidal features at larger distances.

3 STAR FORMATION HISTORIES AND REST-FRAME PHOTOMETRY

In this section, we describe the estimation of star formation histories (SFHs) and rest-frame photometry that are used in Section 4. We compare the observed photometry of each galaxy to a large library of synthetic photometry. The synthetic library is constructed using exponentially-decaying model SFHs, described by five free parameters: the age (T), e-folding timescale (τ), metallicity (Z) and internal extinction (E_{B-V}) of the starburst and the total stellar mass formed (M_*). We vary T between 0.05 Gyrs and the look-back time to $z = 20$ in the rest-frame of the galaxy, τ between 0.01 Gyrs (approximately an instantaneous burst) and 9 Gyrs (approximately constant star formation), Z between $0.05 Z_\odot$ and $2.5 Z_\odot$ and E_{B-V} between 0 and 2 mag. Synthetic photometry is generated for each model SFH by folding it with the stellar models of Charlot & Bruzual (2007) (an updated version of the Bruzual & Charlot (2003) models), through the correct WFC3 and ACS filter throughputs. The empirical law of Calzetti et al. (2000) is used to compute the dust-extincted spectral energy distributions (SEDs). The synthetic library has ~ 2.5 million individual models. Since our galaxies span a large range in redshift ($1 < z < 3$), equivalent libraries are constructed at redshift intervals of $\delta z = 0.01$.

For each galaxy, the values of the free parameters (T , τ , M_* , Z , E_{B-V}) are estimated by comparing its observed photometry to every model in the synthetic library that is closest to it in redshift. The likelihood of each model, $\exp(-\chi^2/2)$, is calculated using the value of χ^2 , computed in the standard way. From the joint probability distribution (which is a function of all five free parameters), each individual parameter is marginalised³ to extract its one-dimensional probability density function (PDF). The median of this PDF is taken as the best estimate of the parameter in question and the 25 and 75 percentile values (which enclose 50% of the probability) are used to calculate an uncertainty on this estimate. The K-corrections required to construct rest-frame photometry for each galaxy are calculated using the best-fit model SED (i.e. where the value of χ^2 is a minimum).

It is worth noting that the accuracy of the derived star formation histories is aided by the availability of photometry covering both the rest-frame UV and optical wavelengths. The rest-frame UV, in particular, offers almost an order of magnitude greater sensitivity to recent star formation than the optical wavelengths (Kaviraj et al. 2007a), and is largely free from the effects of the age-metallicity degeneracy (Kaviraj et al. 2007b). The rest-frame UV colours are therefore a strong indicator of how truly quiescent a galaxy is. While the rest-frame UV photometry constrains the gradual quenching/decline of star formation in our SGs, the rest-frame optical constrains the epoch of stellar mass assembly.

³ The one-dimensional marginalised probability distribution (PD) for age (T), for instance, is obtained from the joint PD by integrating out the other parameters. If $P(T, \tau, M_*, Z, E_{B-V}|D)$ is the joint PD (given the data D), then the marginalised PD for T , $P(T|D) = \int \int \int \int_0^\infty P(T, \tau, M_*, Z, E_{B-V}|D) d\tau dM_* dZ dE_{B-V}$.

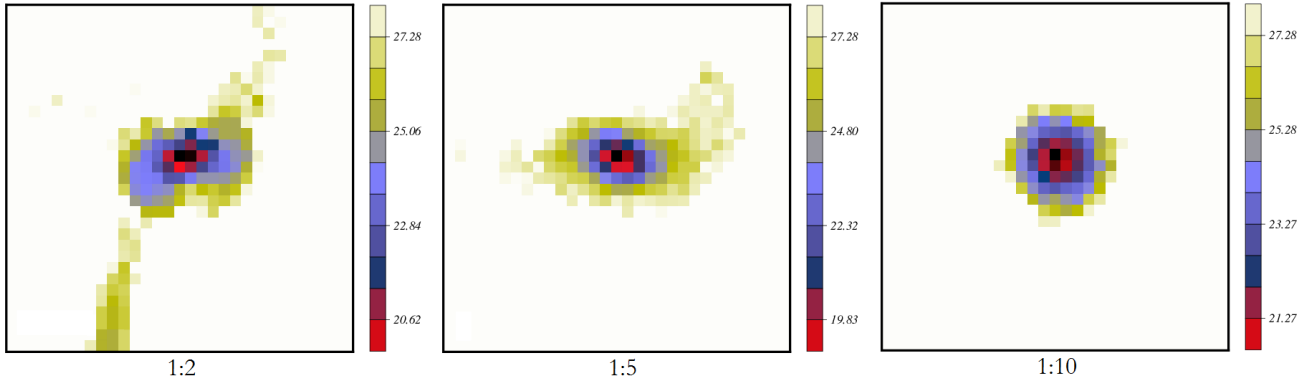


Figure 6. Typical remnants of mergers, drawn from a hydrodynamical cosmological simulation, with mass ratios of 1:2 (left), 1:5 (middle) and 1:10 (right). The colour-coding indicates the surface-brightness (mag arcsec^{-2}) in the H -band (the surface brightness limit of our WFC3/IR images is $\sim 26 \text{ mag arcsec}^{-2}$). To allow comparison with the blue SGs in our sample, the remnants are ‘observed’ while they are in the UV-optical blue cloud, typically $\sim 0.3\text{--}0.4$ Gyr after the merger is complete. The simulations suggest that tidal debris around remnants of mergers that have mass ratios less than $\sim 1:5$ are very unlikely to be observable at the depth of the ERS images across the redshift range considered in this study. In other words, blue SGs that do exhibit such tidal features are likely to be *major-merger remnants* (see text for more details).

4 THE MASS ASSEMBLY OF NEWBORN SPHEROIDS

We begin by exploring the photometric properties of our ERS dataset. Figure 4 presents the *rest-frame* UV-optical colours of the ERS galaxies. The rest-frame NUV wavelengths, based on the GALEX (Martin et al. 2005) NUV filter, are centred at $\sim 2300 \text{ \AA}$. Relaxed and disturbed SGs span the entire colour space occupied by the galaxy population, with $\sim 40\%$ and $\sim 60\%$ of relaxed and disturbed SGs respectively populating the ‘blue cloud’ ($B - V < 0.5$ and $NUV - V < 2.5$). This is consistent with the large range in rest-frame (UVJ) optical colours observed in the massive galaxy population at these redshifts (e.g. Whitaker et al. 2010) and the gradual, rather than abrupt, decline of star formation implied in most massive objects in this redshift range by their spectral features (e.g. Cimatti et al. 2008; van Dokkum & Brammer 2010; Kriek et al. 2011; van Dokkum et al. 2011). In Figure 5 we show the *offset* between the rest-frame colour of individual SGs and that of a dustless, solar-metallicity instantaneous burst at $z = 5$. This comparison, intended only as a guide, indicates that very few of the SGs are consistent with having completed their star formation by $z \sim 5$. Note that, adding the median internal extinction in SGs derived in Section 3 ($E_{B-V} \sim 0.2 \text{ mag}$, see reddening vector in Figure 5) to this instantaneous burst, only reinforces this conclusion. *The star formation in SGs at $1 < z < 3$ is, therefore, either ongoing or recently completed.*

It is worth noting that around half of the SGs that inhabit the blue cloud appear relaxed. Given that tidal features are readily visible in a significant fraction of objects, we explore whether the lack of such features in the *blue relaxed* SGs implies that the star formation in these systems is not being driven by a recent major merger. Indeed, tidal debris from a recent merger is most readily visible in the early stages of relaxation, when star formation remains strong and the galaxy is in the blue cloud (e.g. Carpineti et al. 2012).

To explore the detectability of tidal features in our high-redshift SGs, we appeal to merger remnants of vari-

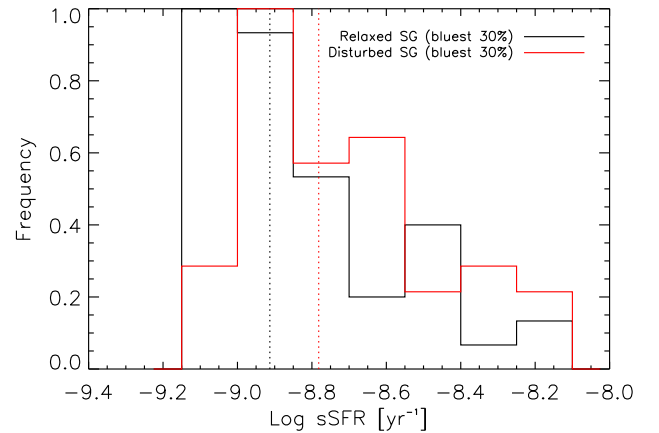


Figure 7. Specific star formation rates (sSFRs) in the bluest 30% of relaxed (black) and disturbed (red) SGs (in the $NUV - r$ colour). Median values are shown using the dotted lines. The general enhancement in sSFR due to a merger appears to be modest, with the median sSFR of the bluest 30% of disturbed SGs being around 0.15 dex ($\sim 40\%$) higher than the corresponding median in their relaxed counterparts. Median values are shown by the dotted vertical lines. Note that the SFR is an average value over the last 10^7 yr.

ous mass ratios drawn from a hydrodynamical cosmological simulation. The simulation, which is described in detail in Peirani (2010), was performed using the GADGET2 code (Springel 2005) with added prescriptions for star formation, feedback from Type Ia and II supernovae, a UV background and metal enrichment. The dark matter and baryonic particle resolutions are $m_{DM} = 7.4 \times 10^6 h^{-1} M_\odot$ and $m_{gas} = m_{star} = 1.5 \times 10^6 h^{-1} M_\odot$ respectively. We refer readers to Section 2.1 of Peirani (2010) for further details of the simulation.

To compare with the blue SGs in our sample, we explore the surface brightness of tidal features in merger remnants at $z \sim 1.25$, the midpoint of the lower redshift bin in Table

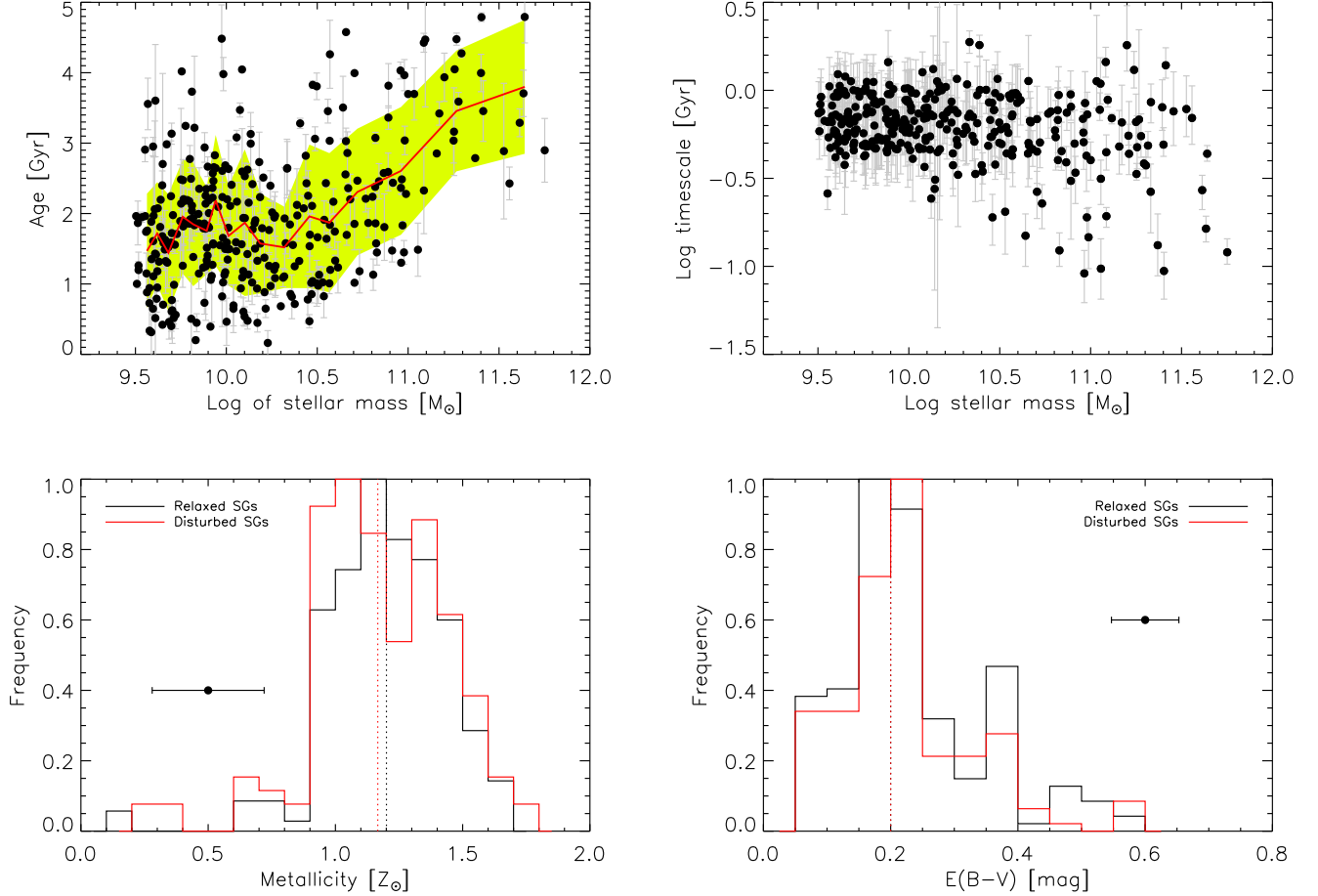


Figure 8. TOP LEFT: Derived starburst age (T) vs. stellar mass in individual SGs. The yellow shaded region in the top-left panel shows a progressive ‘one-sigma’ fit to the data. The red line indicates the mean value, while the yellow shaded area indicates the region that encloses 68% of the galaxies. The typical errors in the stellar masses are better than 0.3 dex. TOP RIGHT: Derived starburst timescale (τ) vs stellar mass in individual SGs. BOTTOM LEFT: Distribution of stellar metallicities in individual SGs. BOTTOM RIGHT: Distribution of internal extinction in individual SGs. Median values are shown using the dotted vertical lines. The error bars in the panels for metallicity and internal extinction indicate average uncertainties in the derived parameters across our SGs.

1. We focus on the lower redshift bin in order to minimise the impact of cosmological dimming - recall that the disturbed SG fraction decreases with redshift in Table 1, plausibly due to cosmological dimming of the tidal features with increasing redshift. In Figure 6 we present typical examples of remnants of mergers that have ratios of 1:2, 1:5 and 1:10. The merger remnants are ‘observed’ while they are in the UV-optical blue cloud (to ensure consistency with our blue observed SGs) and the synthetic images are constructed by combining the simulation outputs with the correct WFC3 filter throughputs, following Peirani et al. (2010). Note that our aim here is to study the surface brightness of *tidal features* around merger remnants and not a detailed exploration of the morphology of the remnants themselves, which would benefit from a simulation with higher resolution.

We find that, while major mergers produce strong features which will be readily visible, mergers with mass ratios of 1:5 are only marginally detectable at $z \sim 1.25$, given the surface-brightness limit of extended objects in our WFC3/IR images (~ 26 mag arcsec $^{-2}$). Mergers with mass

ratios lower than this value (see e.g. 1:10 example in Figure 6) will produce tidal features that will not be visible in our images. At the upper limit of our redshift range ($z \sim 3$), only mergers with mass ratio $\sim 1:2$ will be visible. *In summary, it is likely that only tidal features produced by major mergers are likely to be visible across the redshift range considered in this study.* In other words, if a *blue* SG in our high-redshift sample has experienced a recent *major* merger, then the tidal debris should be visible in the ERS images. The dominant star formation mechanism in the blue relaxed SGs therefore appears unlikely to be a major merger, implying that these systems are driving their star formation via other mechanisms, such as minor mergers, or are the remnants of recently collapsed (cold-stream-fed) clumpy disks, as envisaged in current theoretical work (e.g. Dekel et al. 2009; Elmegreen et al. 2008). Note that minor-merger-driven star formation could, in principle, be distinguished from disk collapse by the presence of tidal features. However, as Figure 6 indicates, our WFC3 images are too shallow to detect tidal debris from minor mergers. While it is challenging to disen-

tangle these two processes using current data, it might be possible to perform this exercise using deeper data, either using the WFC3 itself or from future instruments such as the JWST or the extremely large telescopes.

It is worth noting further that the relaxed SGs in the blue cloud have a similar UV-optical colour distribution in Figure 4 as their disturbed counterparts. Since colours reflect the (average) specific star formation rate (sSFR), this suggests that the sSFR enhancement due to a recent major merger is modest. Figure 7 shows that the median sSFR of the bluest 30% (in the $NUV - r$ colour) of disturbed SGs is around 0.15 dex ($\sim 40\%$) higher than the corresponding median value in their relaxed counterparts. A similarly modest enhancement in sSFR ($\leq 60\%$) due to major mergers has been reported in recent cosmological simulations (Cen 2011) within similar stellar mass and redshift ranges as those studied in this paper. Note that the SFR is an average value over the last 10^7 yr. *Major mergers thus appear relatively insignificant, both in terms of driving the buildup of the SG stellar mass, and enhancing the star formation that is already being driven by other processes e.g. cold-mode accretion and minor mergers.* While our approach is empirical in nature, our conclusions regarding the overall insignificance of major mergers appears consistent with both recent theoretical work (e.g. Cen 2011; Dekel et al. 2009) and an emerging observational literature that indicates a high fraction of systems with disk-like properties (e.g. Shapiro et al. 2008; Stockton et al. 2008; Förster Schreiber et al. 2006) and a remarkably modest incidence of major mergers (see e.g. Genzel et al. 2008; Tacconi et al. 2010, and references therein) amongst star-forming galaxies at $z \sim 2$.

We conclude by summarising the derived star-formation histories of individual SGs. In the top row of Figure 8, we plot the starburst ages (T) and timescales (τ) of individual SGs against their stellar masses. In the bottom row in this figure we show the distributions of metallicities and internal dust extinctions for our SGs. The yellow shaded region in the top-left panel shows a progressive ‘one-sigma’ fit to the data. The red line indicates the mean value, while the yellow shaded area indicates the region that encloses 68% of the galaxies. Individual error bars for each SG are shown and the errors in the galaxy stellar masses are typically better than 0.3 dex.

We find that the star-formation timescales (τ) in SGs are relatively short, with a median of ~ 0.6 Gyr, with uncertainties on individual timescales of ~ 0.3 – 0.4 dex. Given the large uncertainties, timescales as large as ~ 1.5 Gyr cannot be ruled out for most of the individual SGs in our sample. However, the median value for the sample as a whole is smaller than 1 Gyr, consistent with previous measurements of star formation timescales in intermediate and high-redshift SGs (e.g. Ferreras et al. 2004) and the high values of alpha enhancement found in *local* SGs (e.g. Thomas et al. 2005).

In the mass range $10^{9.5} M_\odot < M_* < 10^{10.5} M_\odot$, the starburst timescales (τ) and ages (T) do not correlate strongly with galaxy stellar mass. However, the timescales scatter towards lower values (< 0.3 Gyr) for more massive galaxies ($M_* > 10^{10.5} M_\odot$) and a trend towards increasing age is apparent as we move to systems with higher stellar masses. For example, galaxies at the upper end of our mass range ($M_* > 10^{11.5} M_\odot$) are typically ~ 2 Gyrs older than

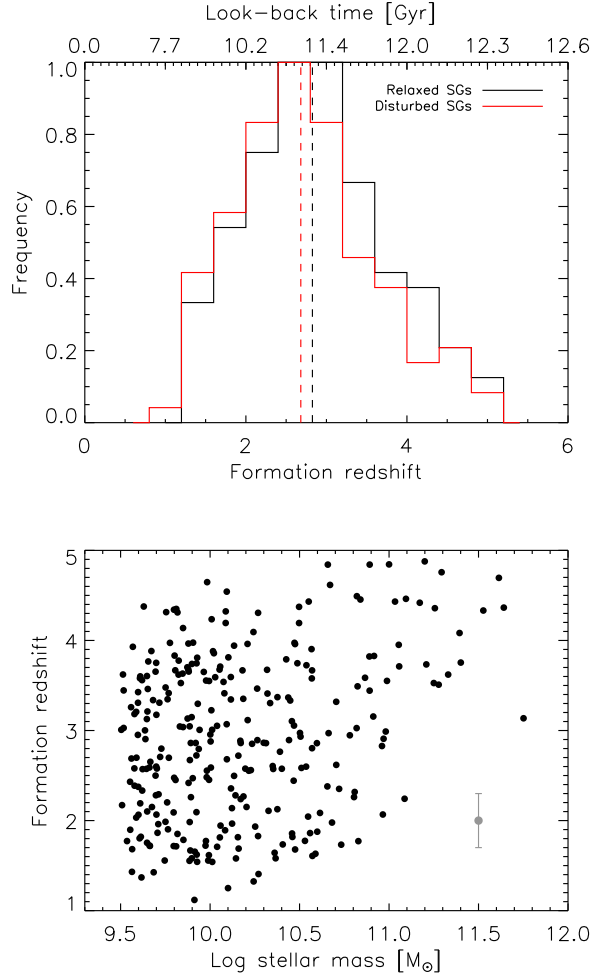


Figure 9. TOP: Histogram of formation redshifts, calculated from the starburst ages (T) and the observed redshifts of the SG population (see text in Section 4 for details). Median values are shown using the dotted vertical lines. Look-back times corresponding to the formation redshifts are indicated on the top x-axis. BOTTOM: Formation redshift vs stellar mass in individual SGs. The error bar indicates the average uncertainty in the formation redshifts across the SG population. The typical errors in the stellar masses are better than 0.3 dex.

their counterparts with masses $\sim 10^{10.5} M_\odot$. These trends are qualitatively consistent with both observational (e.g. Thomas et al. 2005; Juneau et al. 2005) and theoretical evidence (e.g. Neistein et al. 2006; Cattaneo et al. 2008) for ‘downsizing’ in massive galaxies. It is worth noting, however, that a *smooth* downsizing trend with galaxy mass is not observed, and the large scatter in the starburst ages (T) indicate that SGs are not a particularly coeval population. While such coevality has been suggested in the past by the optical colours of local SGs, this is likely due to the fact that 8–10 Gyr of evolution washes out the *details* of the stellar mass assembly. One also has to entertain the possibility that the trends observed in local SGs, between stellar mass and quantities such as luminosity-weighted age, are influenced by late star formation. For example, an identical gas-rich satellite will likely create a larger mass fraction of young stars, and therefore a lower luminosity-weighted age and a larger dilution of $[\alpha/\text{Fe}]$, in a smaller SG.

The median value for the internal dust extinction of our SG sample is $E_{B-V} \sim 0.2$ mag, around a factor of 2 higher than the typical values found in local SGs (Kaviraj et al. 2007a). Super-solar metallicities ($Z > Z_{\odot}$) are favoured, but with significant uncertainties that are typical of this type of photometric parameter estimation. We conclude this section by presenting the ‘formation redshifts’ of the SG population in Figure 9. The formation redshift is calculated using the derived starburst age and observed redshift of the SG in question, i.e. it is the redshift around which the star formation in the galaxy is likely to peak in a WMAP-7 cosmology. The top panel in Figure 8 indicates that the peak of the star formation that builds the SGs in our sample is likely in the redshift range $2 < z < 5$, with a median value of $z \sim 3$. The bottom panel in this figure shows the formation redshifts plotted against the stellar masses for our SGs. The general trends are similar to the plot of age (T) vs stellar mass (top-left panel of Figure 8), with the larger scatter mainly due to the non-linearity between look-back time and redshift.

5 SUMMARY

We have studied ~ 330 newborn spheroidal galaxies (SGs) in the redshift range $1 < z < 3$, to study their high-redshift origin and gain insight into when and how the old stellar populations that dominate today’s Universe formed. SGs have been identified by visual inspection of near-infrared images from the WFC3 Early-Release Science programme, which trace the rest-frame optical wavelengths at these redshifts. Ten-filter HST photometry, covering the rest-frame UV-optical wavelengths, has been used to study the photometric properties of the newborn SG population and empirically estimate their star formation histories.

The rest-frame UV-optical colours of the SG population indicate that virtually none of these galaxies has completed their stellar assembly by $z \sim 5$. The derived star formation histories indicate that the stellar assembly of our SGs likely peaked in the redshift range $2 < z < 5$, with a median value of $z \sim 3$. Given that around half the present-day SG population was in place by $z \sim 1$ (e.g. Bell et al. 2005; Faber et al. 2007), this implies that a significant fraction of the old stars that dominate the local Universe are likely to have formed at these epochs.

Our results show that the star formation episodes that built the massive SGs are relatively short and have decay timescales less than 1.5 Gyr (with a median of ~ 0.6 Gyr). Starburst ages and timescales show no correlation with galaxy stellar mass in the mass range $10^{9.5} M_{\odot} < M_{*} < 10^{10.5} M_{\odot}$. However, the timescales scatter towards lower values (< 0.3 Gyr) for more massive galaxies ($M_{*} > 10^{10.5} M_{\odot}$) and a trend towards increasing age becomes apparent as we move to higher stellar masses, with galaxies that have $M_{*} > 10^{11.5} M_{\odot}$ being ~ 2 Gyrs older than those with $M_{*} < 10^{10.5} M_{\odot}$. However, a *smooth* downsizing trend with galaxy mass is not observed, and the large scatter in the starburst ages indicate that SGs are not a particularly coeval population.

Around half of the SGs in the blue cloud are *relaxed*, i.e. show no morphological disturbances of a recent merger. At the depth of the WFC3 images employed in this study, tidal debris from *major* mergers is likely to be visible at the

epochs probed here. Thus, relaxed SGs in the blue cloud are unlikely to be driving their star-formation episodes via major mergers, suggesting (indirectly) that they may be experiencing minor mergers, or are the remnants of the recent collapse of clumpy disks, in which the star formation has been fed by cold streams (as envisaged in recent theoretical work). Furthermore, those SGs that do show tidal features, and are therefore likely to be recent major-merger remnants, exhibit only modest enhancements in their specific star formation rates of $\sim 40\%$. Thus, major mergers appear relatively insignificant, both in terms of driving the buildup of the SG stellar mass and enhancing the star formation that is already being driven by other processes (e.g. cold-mode accretion, minor mergers.)

This study offers *empirical* insights into the formation of newborn SGs in the early Universe, using the rest-frame optical data that is rapidly becoming available from new space and ground-based surveys. We conclude this paper by outlining several outstanding issues that demand further study. The analysis of very massive galaxies ($M_{*} > 10^{11} M_{\odot}$) requires a larger, statistically-significant sample of objects, such as the complete CANDELS survey, which offers a factor of ~ 20 increase in area compared to the WFC3 ERS programme (but typically in fewer filters compared to the 10-band HST data used here). While we have presented plausible evidence for the general insignificance of major mergers in producing SGs and driving stellar mass growth at high redshift, the role of such mergers in the redshift range $1 < z < 3$ has to be quantified further, by directly comparing the rate of emergence of SGs with the observed major-merger rate. Again, this will benefit from better statistics than is available in either the WFC3 ERS sample or the existing CANDELS data. Bulk visual classification of galaxy morphologies, required for the reliable identification of mergers and SGs (see e.g. Kaviraj et al. 2007a; Kartaltepe et al. 2010) from large datasets such as CANDELS, can be achieved using novel techniques such as the Galaxy Zoo project.

While rest-frame UV/optical photometry provides reasonable constraints on galaxy star formation histories, they can be (significantly) improved using forthcoming panchromatic data. Spectroscopic line indices and/or radio continuum data can put strong priors on stellar/gas-phase metallicities and the current star-formation rate respectively, enabling us to significantly reduce uncertainties on the derived star formation history parameters (c.f. Section 3). Intriguingly, the derived star formation timescales in our SGs appear somewhat longer than those implied by the high $[\alpha/\text{Fe}]$ ratios observed in the low-redshift Universe. However, photometric analyses such as the one performed here typically yield large error bars on the derived timescales, making it difficult to ascertain whether this is a real effect. A systematic study of the stellar/gas-phase metallicities, $[\alpha/\text{Fe}]$ ratios and star formation rates of massive SGs at $z > 1$, using forthcoming spectrographs like KMOS and radio continuum surveys using the SKA precursors (e.g. e-MERLIN), thus becomes a compelling exercise. Looking further ahead, future morphological studies, using the JWST and the extremely large telescopes, will enable us to probe massive galaxies beyond $z > 3$, bridging the gap between SGs at the epoch of peak star formation and their progenitors.

In future papers, we will systematically tackle these is-

sues using the forthcoming datasets mentioned above, both to further our understanding of the emerging SG population and, in particular, to bring such empirical results to bear on our emerging theoretical models for describing the high-redshift Universe.

ACKNOWLEDGEMENTS

We are grateful to the referee Scott Trager for many constructive comments that helped improve the original manuscript. Daniel Thomas, Pieter van Dokkum, Ignacio Ferreras, Mariska Kriek, Claudia Maraston, Simona Mei and Ewan Cameron are thanked for comments and related discussions. SK is grateful for the generous hospitality of the California Institute of Technology, where most of this work was completed. SK also acknowledges fellowships from Imperial College London, the Royal Commission for the Exhibition of 1851 and Worcester College, Oxford.

This paper is based on Early Release Science observations made by the WFC3 Scientific Oversight Committee. We are grateful to the Director of the Space Telescope Science Institute for awarding Director's Discretionary time and deeply indebted to the brave astronauts of STS-125 for rejuvenating HST. Support for HST program 11359 was provided by NASA through grant GO-11359 from the Space Telescope Science Institute, which is operated by the Association of Universities for Research in Astronomy, Inc., under NASA contract NAS 5-26555. R.A.W. also acknowledges support from NASA JWST Interdisciplinary Scientist grant NAG5-12460 from GSFC. The work of AD has been partly supported by the ISF grant 6/08 by GIF grant G-1052-104.7/2009, DIP grant STE1869/1-1.GE625/15-1 and NSF grant AST-1010033.

REFERENCES

- Abraham R. G., Tanvir N. R., Santiago B. X., Ellis R. S., Glazebrook K., van den Bergh S., 1996, *MNRAS*, 279, L47
- Abraham R. G., van den Bergh S., Nair P., 2003, *ApJ*, 588, 218
- Barnes J. E., Hernquist L., 1992, *ARAA*, 30, 705
- Baugh C. M., Cole S., Frenk C. S., 1996, *MNRAS*, 283, 1361
- Bell E. F., Papovich C., Wolf C., et al. 2005, *ApJ*, 625, 23
- Bell E. F., Wolf C., Meisenheimer K., et al. 2004, *ApJ*, 608, 752
- Bernardi M., Sheth R. K., Annis J., et al. 2003, *AJ*, 125, 1882
- Birnboim Y., Dekel A., 2003, *MNRAS*, 345, 349
- Bower R. G., Lucey J. R., Ellis R., 1992, *MNRAS*, 254, 589
- Brammer G. B., van Dokkum P. G., Coppi P., 2008, *ApJ*, 686, 1503
- Bruzual G., Charlot S., 2003, *MNRAS*, 344, 1000
- Bundy K., Ellis R. S., Conselice C. J., 2005, *ApJ*, 625, 621
- Butcher H., Oemler A., 1984, *ApJ*, 285, 426
- Calzetti D., Armus L., Bohlin R. C., Kinney A. L., Koornneef J., Storchi-Bergmann T., 2000, *ApJ*, 533, 682
- Cameron E., Carollo C. M., Oesch P. A., Bouwens R. J., Illingworth G. D., Trenti M., Labbé I., Magee D., 2011, *ApJ*, 743, 146
- Carpinetti A., Kaviraj S., Darg D., Lintott C., Schawinski K., Shabala S., 2012, *MNRAS*, p. 2262
- Cassata P., Cimatti A., Franceschini A., et al. 2005, *MNRAS*, 357, 903
- Cattaneo A., Dekel A., Faber S. M., Guiderdoni B., 2008, *MNRAS*, 389, 567
- Cen R., 2011, *ArXiv e-prints*
- Ceverino D., Dekel A., Bournaud F., 2010, *MNRAS*, 404, 2151
- Ceverino D., Dekel A., Mandelker N., Bournaud F., Burkert A., Genzel R., Primack J., 2012, *MNRAS*, 420, 3490
- Cimatti A., et al. 2008, *A&A*, 482, 21
- Cole S., Lacey C. G., Baugh C. M., Frenk C. S., 2000, *MNRAS*, 319, 168
- Conselice C. J., et al. 2011, *MNRAS*, 413, 80
- Conselice C. J., Bershadsky M. A., Dickinson M., Papovich C., 2003, *AJ*, 126, 1183
- Couch W. J., Barger A. J., Smail I., Ellis R. S., Sharples R. M., 1998, *ApJ*, 497, 188
- Daddi E., et al. 2005, *ApJ*, 626, 680
- de La Rosa I. G., La Barbera F., Ferreras I., de Carvalho R. R., 2011, *MNRAS*, 418, L74
- Dekel A., Birnboim Y., Engel G., Freundlich J., Goerdt T., Mumcuoglu M., Neistein E., Pichon C., Teyssier R., Zinger E., 2009, *Nature*, 457, 451
- Dekel A., Sari R., Ceverino D., 2009, *ApJ*, 703, 785
- Devriendt J., et al. 2010, *MNRAS*, 403, L84
- Ellis R. S., Abraham R. G., Dickinson M., 2001, *ApJ*, 551, 111
- Ellis R. S., Smail I., Dressler A., Couche W. J., Oemler A. J., Butcher H., Sharples R. M., 1997, *ApJ*, 483, 582
- Elmegreen B. G., Bournaud F., Elmegreen D. M., 2008, *ApJ*, 688, 67
- Elmegreen D. M., Elmegreen B. G., Rubin D. S., Schaffer M. A., 2005, *ApJ*, 631, 85
- Faber S. M., Willmer C. N. A., Wolf C., et al. 2007, *ApJ*, 665, 265
- Ferreras I., Lisker T., Carollo C. M., Lilly S. J., Mobasher B., 2005, *ApJ*, 635, 243
- Ferreras I., Lisker T., Pasquali A., Khochfar S., Kaviraj S., 2009, *MNRAS*, 396, 1573
- Ferreras I., Silk J., 2000a, *ApJL*, 541, L37
- Ferreras I., Silk J., 2000b, *ApJ*, 532, 193
- Ferreras I., Silk J., Böhm A., Ziegler B., 2004, *MNRAS*, 355, 64
- Forbes D. A., Ponman T. J., Brown R. J. N., 1998, *ApJ*, 508, L43
- Förster Schreiber N. M., et al. 2006, *ApJ*, 645, 1062
- Franx M., 1995, in van der Kruit P. C., Gilmore G., eds, *IAU Symp. 164: Stellar Populations Measuring the Evolution of the M/L Ratio from the Fundamental Plane*. pp 269–+
- Genzel R., et al. 2008, *ApJ*, 687, 59
- Gialalisco M., et al. 2004, *ApJ*, 600, L93
- Gladders M. D., Lopez-Cruz O., Yee H. K. C., Kodama T., 1998, *ApJ*, 501, 571
- Graves G. J., Faber S. M., Schiavon R. P., 2009, *ApJ*, 693, 486
- Grogin N. A., et al. 2011, *ApJS*, 197, 35
- Hatton S., Devriendt J. E. G., Ninin S., Bouchet F. R., Guiderdoni B., Vibert D., 2003, *MNRAS*, 343, 75
- Hopkins A. M., 2004, *ApJ*, 615, 209

- Hopkins A. M., Beacom J. F., 2006, *ApJ*, 651, 142
- Jogee S., Miller S. H., Penner K., et al. 2009, *ApJ*, 697, 1971
- Jorgensen I., Franx M., Kjaergaard P., 1996, *MNRAS*, 280, 167
- Juneau S., et al. 2005, *ApJL*, 619, L135
- Kartaltepe J. S., et al. 2010, *ApJ*, 721, 98
- Kaviraj S., Devriendt J. E. G., Ferreras I., Yi S. K., 2005, *MNRAS*, 360, 60
- Kaviraj S., Khochfar S., Schawinski K., et al. 2008, *MNRAS*, 388, 67
- Kaviraj S., Rey S., Rich R. M., Yoon S., Yi S. K., 2007a, *MNRAS*, 381, L74
- Kaviraj S., Sohn S. T., O’Connell R. W., Yoon S., Lee Y. W., Yi S. K., 2007b, *MNRAS*, 377, 987
- Kaviraj S., Tan K.-M., Ellis R. S., Silk J., 2011, *MNRAS*, 411, 2148
- Kereš D., Katz N., Fardal M., Davé R., Weinberg D. H., 2009, *MNRAS*, 395, 160
- Kereš D., Katz N., Weinberg D. H., Davé R., 2005, *MNRAS*, 363, 2
- Kocevski D. D., et al. 2012, *ApJ*, 744, 148
- Koekemoer A. M., et al. 2011, *ApJS*, 197, 36
- Komatsu E., et al. 2011, *ApJS*, 192, 18
- Kriek M., van Dokkum P. G., Whitaker K. E., Labbe I., Franx M., Brammer G. B., 2011, *ArXiv e-prints*
- Law D. R., Steidel C. C., Erb D. K., Larkin J. E., Pettini M., Shapley A. E., Wright S. A., 2009, *ApJ*, 697, 2057
- Le Fèvre O., et al. 2004, *A&A*, 417, 839
- Lisker T., 2008, *ApJS*, 179, 319
- Lotz J. M., Primack J., Madau P., 2004, *AJ*, 128, 163
- Lupton R., Blanton M. R., Fekete G., Hogg D. W., O’Mullane W., Szalay A., Wherry N., 2004, *PASP*, 116, 133
- Madau P., Pozzetti L., Dickinson M., 1998, *ApJ*, 498, 106
- Martin D. C., et al. 2005, *ApJ*, 619, L1
- Menanteau F., Abraham R. G., Ellis R. S., 2001, *MNRAS*, 322, 1
- Mignoli M., et al. 2005, *A&A*, 437, 883
- Neistein E., van den Bosch F. C., Dekel A., 2006, *MNRAS*, 372, 933
- Nelan J. E., Smith R. J., Hudson M. J., Wegner G. A., Lucey J. R., Moore S. A. W., Quinney S. J., Suntzeff N. B., 2005, *ApJ*, 632, 137
- Newman A. B., Ellis R. S., Bundy K., Treu T., 2011, *ArXiv e-prints*
- Oke J. B., Gunn J. E., 1983, *ApJ*, 266, 713
- Pasquali A., et al. 2006, *ApJ*, 636, 115
- Peebles P. J. E., 2002, in *ASP Conf. Ser.* 283: A New Era in Cosmology pp 351–+
- Peirani S., 2010, *MNRAS*, 407, 1487
- Peirani S., Crockett R. M., Geen S., Khochfar S., Kaviraj S., Silk J., 2010, *MNRAS*, 405, 2327
- Popesso P., et al. 2009, *A&A*, 494, 443
- Ravikumar C. D., et al. 2007, *A&A*, 465, 1099
- Robaina A. R., Bell E. F., Skelton R. E., et al. 2009, *ApJ*, 704, 324
- Rutkowski M. J., et al. 2012, *ApJS*, 199, 4
- Saglia R. P., Colless M., Baggle G., et al. 1997, in Arnaboldi M., Da Costa G. S., Saha P., eds, *ASP Conf. Ser.* 116: The Nature of Elliptical Galaxies; 2nd Stromlo Symposium The EFAR Fundamental Plane. pp 180–+
- Salim S., Rich R. M., 2010, *ApJL*, 714, L290
- Schiavon R. P., 2007, *ApJS*, 171, 146
- Shapiro K. L., et al. 2008, *ApJ*, 682, 231
- Smith G. P., Treu T., Ellis R. S., Moran S. M., Dressler A., 2005, *ApJ*, 620, 78
- Somerville R. S., Primack J. R., 1999, *MNRAS*, 310, 1087
- Springel V., 2005, *MNRAS*, 364, 1105
- Springel V., Di Matteo T., Hernquist L., 2005, *MNRAS*, 361, 776
- Stanford S. A., Eisenhardt P. R. M., Dickinson M., 1998, *ApJ*, 492, 461
- Stockton A., McGrath E., Canalizo G., Iye M., Maihara T., 2008, *ApJ*, 672, 146
- Strolger L.-G., et al. 2004, *ApJ*, 613, 200
- Szokoly G. P., et al. 2004, *ApJS*, 155, 271
- Tacconi L. J., et al. 2010, *Nature*, 463, 781
- Tal T., Wake D. A., van Dokkum P. G., van den Bosch F. C., Schneider D. P., Brinkmann J., Weaver B. A., 2012, *ApJ*, 746, 138
- Thomas D., Greggio L., Bender R., 1999, *MNRAS*, 302, 537
- Thomas D., Maraston C., Bender R., Mendes de Oliveira C., 2005, *ApJ*, 621, 673
- Toomre A., 1977, in Tinsley B. M., Larson R. B., eds, *Evolution of Galaxies and Stellar Populations* pp 401–+
- Trager S. C., Faber S. M., Dressler A., 2008, *MNRAS*, 386, 715
- Trager S. C., Faber S. M., Worthey G., González J. J., 2000, *AJ*, 119, 1645
- van Dokkum P. G., et al. 2011, *ApJL*, 743, L15
- van Dokkum P. G., Brammer G., 2010, *ApJL*, 718, L73
- Vanzella E., et al. 2008, *A&A*, 478, 83
- Whitaker K. E., et al. 2010, *ApJ*, 719, 1715
- White S. D. M., 1978, *MNRAS*, 184, 185
- Windhorst R. A., et al. 2011, *ApJS*, 193, 27
- Yi S. K., 2003, *ApJ*, 582, 202
- Yi S. K., Yoon S.-J., Kaviraj S., et al. 2005, *ApJ*, 619, L111